Efficient non-doped blue-light-emitting diodes incorporating an anthracene derivative end-capped with fluorene groups

Chen-Hao Wu, Chen-Han Chien, Fang-Ming Hsu, Ping-I Shih and Ching-Fong Shu*

Received 29th September 2008, Accepted 4th December 2008
First published as an Advance Article on the web 27th January 2009
DOI: 10.1039/b817031b

We have synthesized and characterized a novel blue-emitting material, 2-*tert*-butyl-9,10-bis[4′-(9-*p*-tolyl-fluoren-9-yl)biphenyl-4-yl]anthracene (**BFAn**), containing an anthracene core end-capped with 9-phenyl-9-fluorenyl groups. The presence of the sterically congested fluorene groups imparts **BFAn** with a high thermal decomposition temperature (T_d = 510 °C) and results in its forming a stable glass (T_g = 227 °C). Atomic force microscopy measurements revealed that **BFAn** forms high-quality amorphous films and possesses good morphological stability after annealing. Organic light-emitting diodes (OLEDs) featuring **BFAn** as the emitter exhibited an excellent external quantum efficiency of 5.1% (5.6 cd A^{-1}) with Commission Internationale de L'Eclairage coordinates of (0.15, 0.12) that are very close to the National Television Standards Committee's blue standard. The power efficiency of our **BFAn**-based devices reached as high as 5.7 lm W^{-1}, making them superior to other reported non-doped deep-blue OLEDs.

Introduction

Organic light-emitting diodes (OLEDs) have attracted much scientific and commercial attention because of their potential use in high-resolution, full-color, flat-panel displays.[1–5] To meet the requirements for full-color displays, red-,[6,7] green-,[8,9] and blue-emitting[10–12] materials (*i.e.*, the three primary colors) must all feature high electroluminescence (EL) efficiencies, good thermal stabilities, and excellent charge-carrier injection/transport abilities. Although remarkable improvements in OLED performance have been achieved over the past decade, the performance of blue OLEDs is relatively poor in comparison with those of red and green OLEDs. Because of their intrinsically wide band-gap, the synthesis of highly efficient blue-light emitters exhibiting good color purity remains a great challenge for the development of new OLEDs.

Anthracene derivatives have been studied extensively and developed as blue-light-emitting materials in OLEDs because of their excellent photoluminescence (PL) and electroluminescence (EL) properties.[13–20] Among these derivatives, 9,10-diphenylanthracene (DPA) is an attractive material for its unity fluorescence quantum efficiency in dilute solution and high fluorescence in the solid state. Unfortunately, DPA tends to crystallize in the solid state,[21,22] thereby limiting its OLED applications because crystal formation destroys film homogeneity and raises the resistance of the sample, ultimately leading to device failure.[23] In general, amorphous thin films (in OLEDs) having high glass transition temperatures (T_g) are less vulnerable to heat and, hence, their devices perform more stably.[24–27] Consequently, light-emitting materials possessing high values of T_g are required to retain the film morphology during the operation of the device.

In this study, we developed a highly efficient blue-emitting material, 2-*tert*-butyl-9,10-bis[4′-(9-*p*-tolylfluoren-9-yl)biphenyl-4-yl]anthracene (**BFAn**), possessing high thermal stability and good amorphous film-formation capability. This new blue emitter contains an anthracene core and two end-capping fluorene groups, the 3D cardo structures of which improve the molecular rigidity and mitigate the close-packing of molecules in the solid state, leading to an amorphous organic thin film displaying pronounced morphological stability.[28] We fabricated non-doped blue-light OLEDs incorporating **BFAn** to evaluate its applicability. A device incorporating **BFAn** as the emitter and 2-*tert*-butyl-9,10-bis[4′-(1-phenylbenzoimidazyl)biphenyl-4-yl] anthracene (**BIAn**) as the electron-transporting layer exhibited a high external quantum efficiency of 5.1% (5.6 cd A^{-1}) and an excellent power efficiency (5.7 lm W^{-1} at 7.8 mA cm^{-2}), together with satisfactory Commission Internationale de L'Eclairage (CIE) coordinates (0.15, 0.12). To the best of our knowledge, this power efficiency is among the best ever reported for fluorescent blue-light-emitting OLEDs.[13–20,29–33]

Results and discussion

Synthesis

Scheme 1 illustrates the synthetic route we used to prepare the anthracene derivative **BFAn** presenting two fluorene terminal groups. The acid-promoted Friedel–Crafts-type substitution of toluene with 9-(4-bromophenyl)-fluoren-9-ol (**1**) afforded the bromide **2**, which in turn underwent cross-coupling with the pinacol ester of diboron to give the arylboronic ester **3**.[34] We prepared 2-*tert*-butyl-9,10-bis(4-bromophenyl)anthracene (**6**) using a procedure reported previously: the reaction of monolithiated 1,4-dibromobenzene with 2-*tert*-butylanthraquinone and then reduction of the intermediate diol with potassium iodide and sodium hypophosphite in acetic acid.[15] Suzuki coupling of the boronic ester **3** and the dibromide **6** yielded the target compound **BFAn**. The ^{1}H and ^{13}C NMR spectra, high-resolution mass spectrum, and elemental analysis (EA) were consistent with the proposed molecular structure of **BFAn**.

Department of Applied Chemistry, National Chiao Tung University, Hsin-Chu, Taiwan, 30050

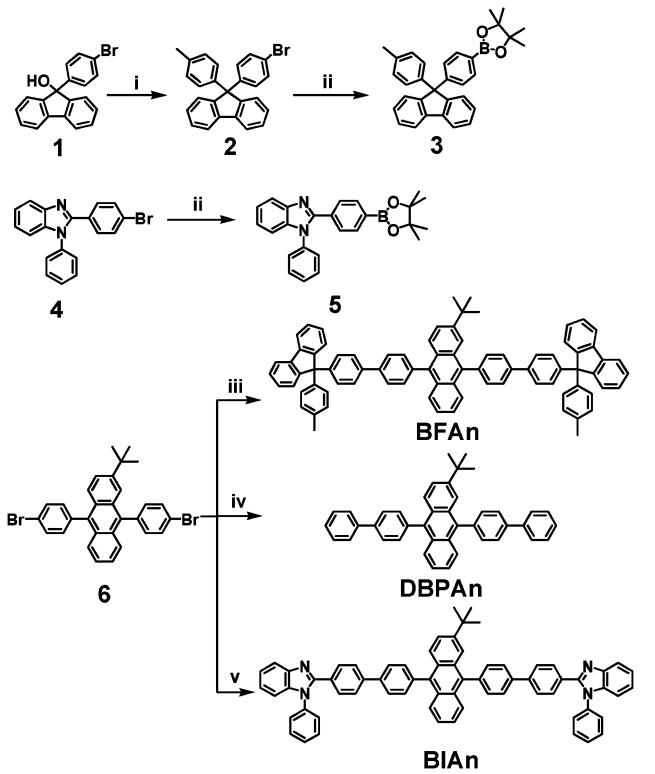

Scheme 1 *Reagents*: (i) CF_3SO_3H, toluene; (ii) bis(pinacolato)diboron, $Pd(dppf)Cl_2$, KOAc, DMF; (iii) **3**, $Pd(PPh_3)_4$, K_2CO_3, toluene/H_2O, Aliquat 336; (iv) phenylboronic acid, $Pd(PPh_3)_4$, K_2CO_3, toluene/H_2O, Aliquat 336; (v) **5**, $Pd(PPh_3)_4$, K_2CO_3, toluene/H_2O, Aliquat 336.

Thermal properties

We investigated the thermal properties of **BFAn** using differential scanning calorimetry (DSC) and thermogravimetric analysis (TGA). Fig. 1a displays DSC curves of **BFAn** recorded over the temperature range 50–400 °C. The sublimated sample melted at 391 °C on the first heating only, and then it transformed into a glassy state upon cooling from the melt. When we heated the amorphous glassy sample again, a glass transition (T_g) occurred at 227 °C; we observed no exothermic peak due to crystallization at temperatures up to 400 °C. This relatively high value of T_g, which suggests potentially enhanced device stability, is a very desirable feature for emissive materials in light-emitting applications. To verify the role played by the fluorene terminal units in determining the thermal behavior of **BFAn**, we prepared the corresponding anthracene derivative lacking fluorene end-capping groups (**DBPAn**, Scheme 1) as a reference compound. **DBPAn** exhibits its glass transition at 126 °C, followed by a broad crystallization feature at 176 °C and a well-defined melting point at 293 °C (Fig. 1b). These observations indicate that the enhanced thermal stability of the amorphous glass state of **BFAn** can be attributed to the presence of its rigid fluorene end-groups and its high molecular weight. In addition, **BFAn** possesses excellent thermochemical stability, as evidenced through TGA, with its 5% weight loss temperature under nitrogen atmosphere being 510 °C. In contrast, **DBPAn** exhibits inferior thermal stability; its 5% weight loss temperature is 343 °C.

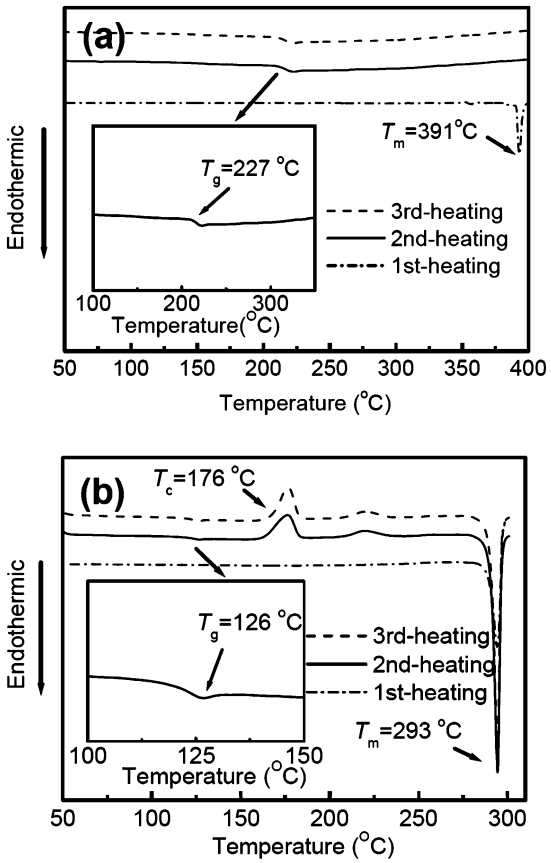

Fig. 1 DSC traces of (a) **BFAn** and (b) **DBPAn** (heating rate: 20 °C min^{-1}). Insets: Expanded views of the second DCS heating scans of (a) **BFAn** (100–350 °C) and (b) **DBPAn** (100–150 °C). T_c: crystallization temperature; T_g: glass-transition temperature; T_m: melting-point temperature.

To further investigate the morphological stabilities of **BFAn** and **DBPAn**, we used vapor deposition to prepare thin films of each of these materials on silicon wafer substrates and then used atomic force microscopy (AFM) to determine their surface morphologies. After vapor deposition, we performed an annealing process involving heating the films at 120 °C for 10 h under a nitrogen atmosphere and then cooling to room temperature. The topographical images in Fig. 2 reveal that **BFAn** provided a uniform surface that underwent no morphological changes after annealing. The root-mean-square (RMS) roughnesses of the pristine and annealed film were 0.31 and 0.32 nm, respectively. In contrast, thermal annealing induced crystallite formation in the **DBPAn** film, as indicated by changes in the surface morphology; the RMS roughness of this annealed film was 40.1 nm, *ca.* 100-fold higher than that of the film prior to annealing (0.35 nm). These images provide further evidence that the thermal stability of **BFAn** is greater than that of **DBPAn**, presumably because the presence of the fluorene end-capping groups hinders the close packing of **BFAn** and suppresses its crystallizability, resulting in an amorphous material exhibiting pronounced morphological stability.

Photophysical properties

The photophysical data of **BFAn** and **DBPAn** are summarized in Table 1. The UV–Vis absorptions of **BFAn** and **DBPAn** showed

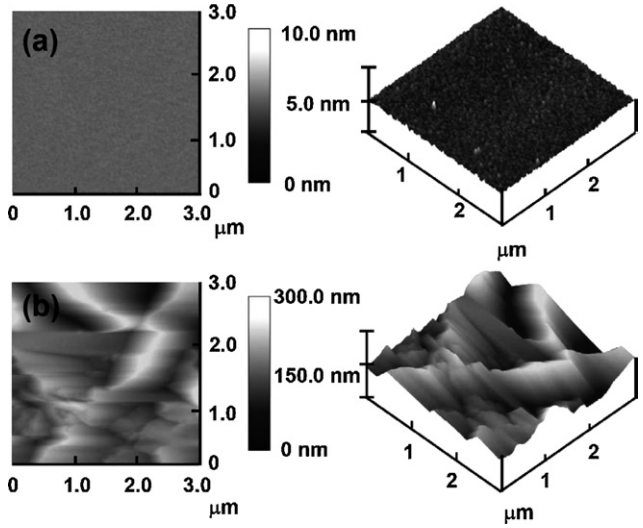

Fig. 2 AFM images (top and angled views) of (a) **BFAn** and (b) **DBPAn** layers, after annealing at 120 °C for 10 h under a nitrogen atmosphere.

the characteristic vibrational patterns of the isolated anthracene core ($\lambda_{max} = 358$, 378, and 398 nm for **BFAn** and $\lambda_{max} = 356$, 376 and 398 nm for **DBPAn**).[21,35] In addition, we assigned the absorption bands of **BFAn** in the region from 290 to 320 nm to the peripheral fluorene groups ($\lambda_{max} = 289$, 299, and 311 nm).[36] Upon excitation at 365 nm, the solutions of **BFAn** and **DBPAn** exhibited blue emissions having an emission maximum at 446 and 431 nm, respectively. Fig. 3 presents the absorption and photoluminescence (PL) spectra of **BFAn** in dilute toluene solution and as a solid film on a quartz plate. The absorption and emission spectra of the **BFAn** thin film were similar to those acquired in dilute solution, but with slight red-shifts (3 and 4 nm, respectively). These small spectral shifts in the solid state spectra without the appearance of the excimer emission imply that the intermolecular interactions were weak, *i.e.*, they were restrained effectively by the bulky end-capping fluorene groups. We calculated the fluorescence quantum yield (Φ_f) of **BFAn** in the dilute toluene solution to be 0.93, using DPA ($\Phi_f = 0.90$ in cyclohexane) as a calibration standard. In addition, we used an integrating sphere apparatus to measure the solid state quantum yield ($\Phi_f = 0.84$) on a quartz plate. The high quantum yields of **BFAn** make it an excellent candidate for use as an efficient blue-light-emitting material in OLEDs.

Electroluminescence properties of OLEDs

To evaluate the applicability of using **BFAn** as the emitting layer (EML), we fabricated two non-doped blue-emitting devices

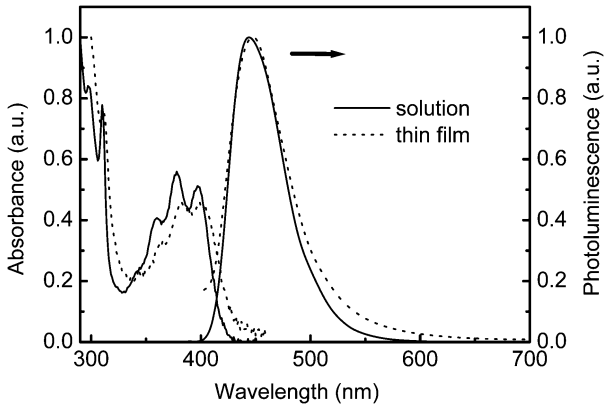

Fig. 3 UV–Vis absorption and PL spectra of **BFAn** in dilute toluene solution and in the solid state.

(I and II) through sequential vapor deposition of the materials onto ITO glass under vacuum (3×10^{-6} torr). Device I had the following configuration: indium tin oxide (ITO)/4,4′-bis[*N*-(1-naphthyl)-*N*-phenylamino]biphenyl (NPB) (20 nm)/4,4′,4″-tris(*N*-carbazolyl)triphenylamine (TCTA) (10 nm)/**BFAn** (40 nm)/1,3,5-tris(*N*-phenylbenzimidazol-2-yl)benzene (TPBI) (40 nm)/LiF (1 nm)/Al (100 nm). Fig. 4 displays the device structure and relative HOMO/LUMO energy levels of the materials used in this study. We determined the HOMO energy level of **BFAn** (−5.85 eV) using an AC-2 photoelectron spectrometer; we estimated the LUMO energy level (−2.92 eV) by adding the optical energy gap to the obtained HOMO energy level. NPB and TCTA were employed as bilayer hole-transporting layers (HTLs) to provide cascade hole injection and transport; TCTA also functioned as an effective electron/exciton blocker; TPBI was used as both the electron-transporting layer (ETL) and a hole-blocker. Device I exhibited a maximum external quantum efficiency as

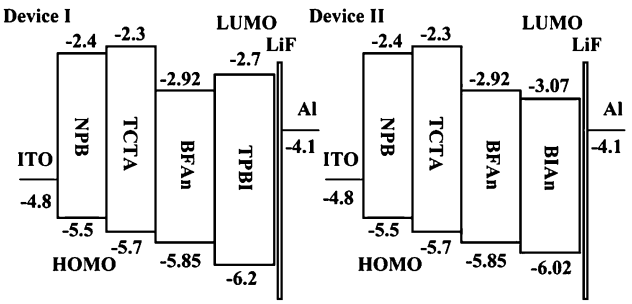

Fig. 4 Relative HOMO/LUMO energy levels of the materials used in devices I and II.

Table 1 Physical properties of the anthracene derivatives

Compound	UV λ_{max} (nm)[a]	PL λ_{max} (nm)[a]	HOMO (eV)[b]	LUMO (eV)[c]	T_g (°C)	T_m (°C)	T_d (°C)[d]
BFAn	289, 299, 311, 358, 378, 398	446	−5.85	−2.92	227	391	510
DBPAn	356, 376, 398	431	−5.76	−2.82	126	293	343
BIAn	316, 378, 398	438	−6.02	−3.07	192	355	502

[a] Measured in dilute toluene solution. [b] Determined using a photoelectron spectrometer (AC-2). [c] Estimated by adding the optical energy gap to the obtained HOMO energy level. [d] Temperature at which a 5% weight loss was detected.

high as 5.0% (5.5 cd A^{-1}, 5.0 lm W^{-1}) at 2.0 mA cm^{-2} with a brightness of 110 cd m^{-2}. Even at a much higher brightness of 1000 cd m^{-2}, the external quantum efficiency and power efficiency remained high at 4.6% and 3.6 lm W^{-1}, respectively. These values reveal that **BFAn** exhibits potential for practical use in display applications. For the purpose of comparison, we also fabricated a reference device using a conventional blue-emitting material, 9,10-di-(2-naphthyl)anthracene (ADN), as the EML. The control ADN-based device showed inferior EL performance with maximum efficiencies of 2.9% and 1.9 lm W^{-1}, which were similar to the reported values of other ADN-based devices.[37–39]

In the case of device II, we replaced TPBI with a novel ETL material, 2-*tert*-butyl-9,10-bis[4′-(1-phenylbenzoimidazyl)biphenyl-4-yl]anthracene (**BIAn**, Scheme 1), which has a lower LUMO (−3.07 eV, Table 1) than that of TPBI (−2.7 eV), to facilitate electron injection from the cathode to the organic layer. Fig. 5 displays typical current density–voltage–luminance (*I–V–L*) characteristics of devices I and II. At the same driving voltage, device II exhibits a higher current density and enhanced brightness relative to those of device I. Fig. 6 reveals that device II displays improved EL performance in comparison with that of device I; its maximum external quantum efficiency reached 5.1% (5.6 cd A^{-1}, 5.0 lm W^{-1}) at 7.8 mA cm^{-2} with a brightness of 436 cd m^{-2}. The efficiency of device II decreased only slightly to 4.7% (5.2 cd A^{-1}, 4.1 lm W^{-1}) at a higher luminance of 1000 cd m^{-2}. Table 2 summarizes the EL performance of these two **BFAn**-based devices.

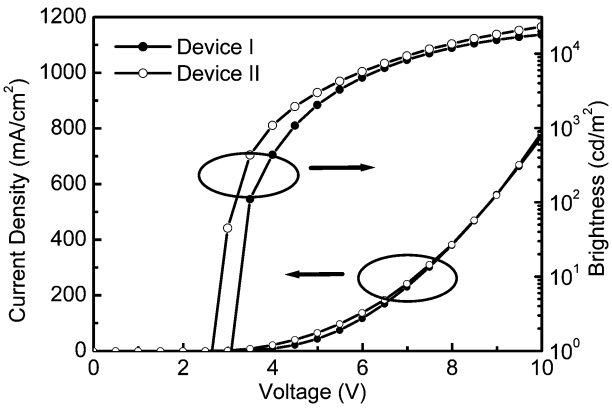

Fig. 5 *I–V–L* characteristics of devices I and II.

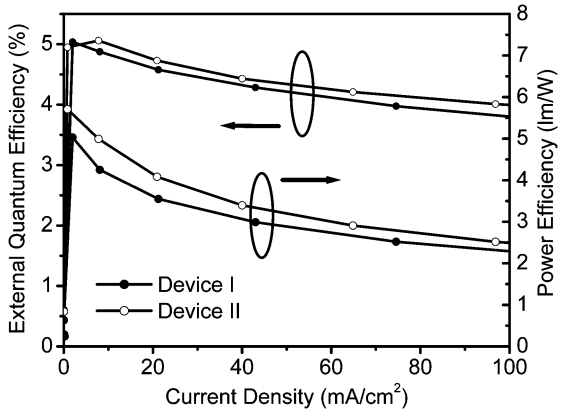

Fig. 6 External quantum efficiency and power efficiency of devices I and II plotted as functions of the current density.

Table 2 EL performance of devices I–II

	I	II
Voltage (V)[a]	3.0	2.5
Brightness (cd m^{-2})[b]	530 (4183)	543 (4382)
E.Q.E. (%)[b]	4.8 (3.8)	5.0 (4.0)
L.E. (cd A^{-1})[b]	5.4 (4.2)	5.5 (4.4)
P.E. (lm W^{-1})[b]	4.2 (2.3)	4.8 (2.5)
Max. E.Q.E. (%)	5.0	5.1
Max. L.E. (cd A^{-1})	5.5	5.6
Max. P.E. (lm W^{-1})	5.0	5.7
EL λ_{max} (nm)[c]	450	450
CIE (x, y)[c]	(0.15, 0.12)	(0.15, 0.12)

[a] Recorded at 1 cd m^{-2}. [b] At 10 mA cm^{-2}, the data in the parentheses were taken at 100 mA cm^{-2}. [c] At 7 V.

The turn-on voltage (corresponding to 1 cd m^{-2}) decreased from 3.0 V for device I to 2.5 V for device II, leading to the higher power efficiency of device II (5.7 lm W^{-1}; Fig. 6). We attribute this enhancement to the better electron injection from the LiF/Al electrode to **BIAn** than to TPBI. To verify this hypothesis, we constructed electron-only devices to investigate the injection of electrons from the cathode to the organic layer. These electron-only devices had the configuration ITO/2,9-dimethyl-4,7-diphenyl-1,10-phenanthroline (BCP) (30 nm)/TPBI or **BIAn** (60 nm)/LiF (1 nm)/Al (100 nm). Because of the lower HOMO energy level of BCP (−6.5 eV), no hole injection occurred from the anode to the organic layers. Because only electrons could be injected from the cathode to the organic layers, electrons dominated the measured current density–voltage (*I–V*) characteristics. As indicated in Fig. 7, the electron-only device incorporating **BIAn** had a much higher injection current relative to that of the TPBI-based device, suggesting that the energy barrier for electron injection from the cathode to the **BIAn** layer was considerably lower than that to the TPBI layer. Consequently, the use of **BIAn** facilitated effective electron injection, resulting in the higher power efficiency of device II.

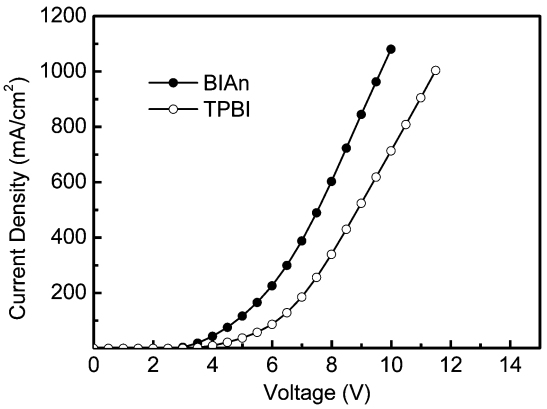

Fig. 7 *I–V* curves of the electron-only devices.

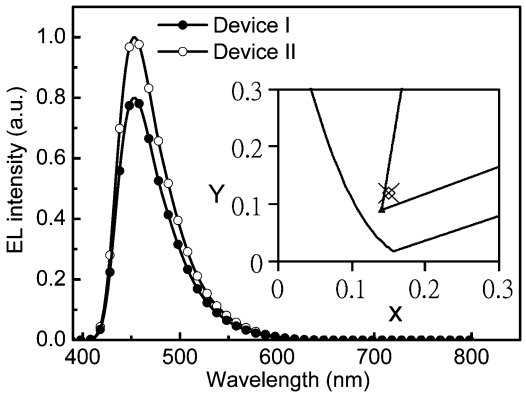

Fig. 8 EL spectra of devices I and II operated at 7 V. Inset: CIE coordinates of devices I (diamond) and II (cross).

The EL spectra of devices I and II display deep-blue emissions with maxima centered at 450 nm (Fig. 8). These EL spectra are quite similar to the PL spectrum of **BFAn** in the solid state (Fig. 3), indicating that all of the emissions originate exclusively from the **BFAn** layer. The inset to Fig. 8 provides the corresponding CIE coordinates of devices I and II; the CIE chromaticity coordinates of (0.15, 0.12) are very close to the standard blue emission recommended by the National Television Standards Committee (NTSC). Furthermore, the emission color of devices I and II remained almost constant under the different bias conditions. The corresponding CIE coordinates changed only slightly, from (0.15, 0.11) at 5.0 V (43 mA/cm^2, 2042 cd/m^2) to (0.15, 0.12) at 9.0 V (562 mA/cm^2, 15314 cd/m^2) for device I and from (0.15, 0.11) at 5.0 V (65 mA/cm^2, 3000 cd/m^2) to (0.15, 0.12) at 9.0 V (560 mA/cm^2, 18191 cd/m^2) for device II. This result demonstrated that **BFAn** was a promising blue OLEDs material with good color stability.

Conclusion

We have fabricated highly efficient non-doped deep-blue OLEDs incorporating the anthracene derivative **BFAn**, a blue-emitting material featuring phenyl-substituted fluorene end-capping groups that enhance its thermal and morphological stabilities while maintaining the excellent fluorescence quantum yield of the anthracene core. The **BFAn**-based non-doped devices exhibit satisfactory blue emissions having CIE coordinates located at (0.15, 0.12), very close to the NTSC's standard blue CIE coordinates. Moreover, the **BFAn**-based devices exhibit outstanding efficiencies, with maximum values of external quantum efficiency reaching as high as 5.1% (5.6 cd A^{-1}) at 7.8 mA cm^{-2}. Notably, the power efficiency of device II (5.7 lm W^{-1}) is superior to those of previously reported blue OLEDs.[41–43]

Experimental

General information

9-(4-Bromophenyl)-fluoren-9-ol (**1**)[36] and 2-(4-bromophenyl)-1-phenylbenzoimidazole (**4**)[44] were synthesized as reported previously. The solvents were dried using standard procedures. All reagents were used as received from commercial sources, unless otherwise stated. The ^{1}H and ^{13}C NMR spectra were recorded on Bruker-DRX 300 MHz spectrometers. Mass spectra were obtained using a JEOL JMS-HX 110 mass spectrometer. DSC was performed using a SEIKO EXSTAR 6000DSC unit at heating and cooling rates of 20 and 50 °C min^{-1}, respectively. Samples were scanned from 50 to 400 °C, cooled to 0 °C, and then scanned again from 50 to 400 °C. The values of T_g were determined from the second heating scan. TGA was performed using a DuPont TGA 2950 instrument. The thermal stability of the samples under a nitrogen atmosphere was determined by measuring their weight loss while heating at a rate of 20 °C min^{-1}. UV–Vis spectra were measured using an HP 8453 diode-array spectrophotometer. PL spectra were obtained using a Hitachi F-4500 luminescence spectrometer. The HOMO energy levels of organic thin films were measured using a Riken-Keiki AC-2 photoelectron spectrometer; the LUMO energy levels of materials were estimated by subtracting the optical energy gap from the measured HOMO energy level. AFM images were recorded under ambient conditions using a Digital Nanoscope IIIa instrument operated in the tapping mode.

9-(4-Bromophenyl)-9-*p*-tolylfluorene (2)

A mixture of **1** (2.00 g, 5.95 mmol), toluene (20 mL), and CF_3SO_3H (5 mL) was stirred for 4 h at 25 °C under nitrogen. The reaction mixture was then treated with saturated $NaHCO_{3(aq)}$ and extracted with EtOAc. The organic extracts were dried ($MgSO_4$) and the solvent evaporated under vacuum. The crude product was purified through column chromatography (*n*-hexane) to give **2** (1.95 g, 80%). ^{1}H NMR (300 MHz, $CDCl_3$): δ 7.76 (d, $J = 8.1$ Hz, 2H), 7.37–7.26 (m, 8H), 7.07 (d, $J = 8.7$ Hz, 2H), 7.06 (d, $J = 8.1$ Hz, 2H), 7.05 (d, $J = 6.3$ Hz, 2H), 2.29 (s, 3H). ^{13}C NMR (75 MHz, $CDCl_3$): δ 151.4, 145.8, 142.8, 140.6, 136,9, 131.7, 130.4, 129.6, 128.7, 128.4, 128.4, 128.1, 126.5, 121.2, 120.8, 65.2, 21.5. MS (EI) *m*/*z* 410.

9-[4-(4,4,5,5-Tetramethyl-1,3,2-dioxaborolan-2-yl)phenyl]-9-*p*-tolylfluorene (3)

A solution of **2** (1.95 g, 4.76 mmol), 4,4,4′,4′,5,5,5′,5′-octamethyl-2,2′-bis(1,3,2-dioxaborolane) (1.33 g, 5.23 mmol), KOAc (1.39 g, 14.2 mmol), and [1,1′-bis(diphenylphosphino)ferrocene]dichloropalladium(II) [Pd(dppf)Cl_2, 15 mg] in anhydrous DMF (25 mL) was deoxygenated by purging with N_2 and then it was heated at 85 °C under N_2. After 12 h, the reaction mixture was cooled to room temperature, mixed with water (50 mL), and extracted with CH_2Cl_2 (3 × 50 mL). The combined organic phases were dried ($MgSO_4$) and concentrated under reduced pressure. The crude product was purified through column chromatography (*n*-hexane/EtOAc, 12:1) to give **3** (1.67 g, 76%). ^{1}H NMR (300 MHz, $CDCl_3$): δ 7.78 (d, $J = 7.2$ Hz, 2H), 7.69 (d, $J = 8.1$ Hz, 2H), 7.40–7.37 (m, 5H), 7.34–7.23 (m, 4H), 7.10–7.06 (m, 4H), 2.31 (s, 3H), 1.33 (s, 12H). ^{13}C NMR (75 MHz, $CDCl_3$): δ 151.5, 149.7, 143.2, 140.6, 136.7, 135.1, 129.3, 128.4, 128.2, 127.8, 120.5, 84.1, 65.8, 25.2, 21.4. MS (EI) *m*/*z* 458.

1-Phenyl-2-[4-(4,4,5,5-tetramethyl-1,3,2-dioxaborolan-2-yl)phenyl]benzoimidazole (5)

According to the procedure described for **3**, the reaction of 2-(4-bromophenyl)-1-phenylbenzoimidazole (**4**, 1.50 g, 4.31 mmol),

4,4,4′,4′,5,5,5′,5′-octamethyl-2,2′-bis(1,3,2-dioxaborolane) (1.20 g, 4.73 mmol), KOAc (1.26 g, 12.9 mmol), $Pd(dppf)Cl_2$ (15 mg), and DMF (30 mL) gave **5** as a white solid (1.15 g, 67.6%). ^{1}H NMR (300 MHz, $CDCl_3$): δ 7.83 (d, $J = 7.8$ Hz, 1H), 7.66 (d, $J = 8.3$ Hz, 2H), 7.49 (d, $J = 8.3$ Hz, 2H), 7.41–7.37 (m, 3H), 7.27–7.15 (m, 5H), 1.25 (s, 12H). ^{13}C NMR (75 MHz, $CDCl_3$): δ 152.6, 143.3, 137.3, 135.0, 130.3, 129.0, 128.9, 127.8, 123.9, 120.3, 110.9, 84.4, 25.3. MS (FAB) *m/z* 397 [M + 1].

2-*tert*-Butyl-9,10-bis[4′-(9-*p*-tolylfluoren-9-yl)biphenyl-4-yl]anthracene (BFAn)

Aqueous K_2CO_3 (2.0 M, 10 mL) was added to a solution of **3** (1.67 g, 3.64 mmol), 9,10-bis(4-bromophenyl)-2-*tert*-butylanthracene (**6**, 1.00 g, 1.84 mmol), and Aliquat 336 (*ca.* 220 mg) in toluene (60 mL). The reaction mixture was degassed and then tetrakis(triphenylphosphine)palladium [$Pd(PPh_3)_4$, *ca.* 25 mg] was added under a flow of nitrogen. The reaction mixture was then heated at 85 °C while stirring under nitrogen. After 10 h, the reaction mixture was cooled to room temperature and then poured into aqueous 70% MeOH (80 mL). The precipitate was collected by filtration, washed with MeOH, and dried under vacuum. The crude product was purified through column chromatography (*n*-hexane/EtOAc, 12:1) to afford **BFAn** (1.23 g, 65%) as a yellow powder. ^{1}H NMR (300 MHz, $CDCl_3$): δ 7.85–7.79 (m, 12H), 7.74–7.62 (m, 5H), 7.58–7.49 (m, 8H), 7.42–7.32 (m, 14H), 7.21 (dd, $J = 8.2$ Hz, 1.5 Hz, 4H), 7.11 (d, $J = 6.6$ Hz, 4H), 2.36 (s, 6H), 1.31 (s, 9H). ^{13}C NMR (75 MHz, $CDCl_3$): δ 151.3, 147.3, 145.4, 145.3, 142.9, 142.8 140.2, 139.7, 139.4, 139.0, 138.1, 136.5, 136.3, 131.7, 130.9, 130.1, 129.9, 129.6, 129.0, 128.7, 128.6, 128.5, 128.1, 128.0, 127.8, 127.7, 127.4, 126.9, 126.8, 126.2, 124.8, 124.6, 121.1, 65.0, 34.9, 31.2, 20.9. MS (FAB) *m/z* 1047 [M + 1]. HRMS (FAB) calcd. for $C_{82}H_{63}$ $[M + H]^+$ *m/z* 1047.4852; found 1047.4932. Anal. Calcd for $C_{82}H_{63}$: C, 94.03; H, 5.97. Found: C, 93.77; H, 6.09%.

9,10-Bis(biphenyl-4-yl)-2-*tert*-butylanthracene (DBPAn)

Aqueous K_2CO_3 (2.0 M, 10 mL) was added to a solution of phenylboronic acid (0.44 g, 3.61 mmol), 9,10-bis(4-bromophenyl)-2-*tert*-butylanthracene (**6**, 1.00 g, 1.84 mmol), and Aliquat 336 (*ca.* 220 mg) in toluene (40 mL). The reaction mixture was degassed and then $Pd(PPh_3)_4$ (*ca.* 15 mg) was added under a flow of nitrogen. The reaction mixture was heated at 85 °C while stirring under nitrogen. After 10 h, the mixture was cooled to room temperature and then poured into aqueous 50% MeOH (80 mL); the yellow precipitate was filtered, washed with MeOH and dried under vacuum. The crude product was purified through column chromatography (*n*-hexane/EtOAc, 12:1) to afford **DBPAn** (0.68 g, 68.7%) as a yellowish powder. ^{1}H NMR (300 MHz, $CDCl_3$): δ 7.91–7.72 (m, 12H), 7.62–7.52 (m, 9H), 7.49–7.42 (m, 2H), 7.39–7.35 (m, 2H), 1.31 (s, 9H). ^{13}C NMR (75 MHz, $CDCl_3$): δ 147.8, 141.3 140.6, 140.4, 138.7, 138.6, 136.9, 136.7, 132.2, 132.1, 130.5, 130.3, 129.3, 127.6, 127.5, 127.3, 125.1, 125.0, 121.6, 35.4, 31.2. MS (FAB) *m/z* 539 [M + 1]. HRMS (FAB) calcd. for $C_{42}H_{35}$ $[M + H]^+$ *m/z* 539.2661; found 539.2741. Anal. Calcd for $C_{42}H_{34}$: C, 93.64; H, 6.36. Found: C, 93.67; H, 6.36%.

2-*tert*-Butyl-9,10-bis[4′-(1-phenylbenzoimidazyl)biphenyl-4-yl]anthracene (BIAn)

Aqueous K_2CO_3 (2.0 M, 10 mL) was added to a solution of **5** (0.70 g, 1.76 mmol), 9,10-bis(4-bromophenyl)-2-*tert*-butylanthracene (**6**, 0.48 g, 0.89 mmol), and Aliquat 336 (*ca.* 220 mg) in toluene (40 mL). The reaction mixture was degassed and then $Pd(PPh_3)_4$ (*ca.* 15 mg) was added under a flow of nitrogen. The reaction mixture was heated at 85 °C while stirring under nitrogen. After 10 h, the mixture was cooled to room temperature and then poured into aqueous 50% MeOH methanol (80 mL); the yellow precipitate was filtered, washed with MeOH, and dried under vacuum to provide a crude product that was purified through column chromatography (*n*-hexane/EtOAc, 8:1) to give **BIAn** (0.54 g, 65.8%) as a yellowish powder. ^{1}H NMR (300 MHz, $CDCl_3$): δ 7.94 (d, $J = 7.8$ Hz, 2H), 7.87–7.77 (m, 9H), 7.72–7.69 (m, 12H), 7.66–7.59 (m, 5H) 7.51–7.49 (m, 8H), 7.45–7.31 (m, 5H), 1.28 (s, 9H). ^{13}C NMR (75 MHz, $CDCl_3$): δ 152.5, 147.9 143.4, 142.1, 139.4, 139.3, 137.7, 137.5, 136.8, 136.6, 132.3, 130.0, 129.9, 129.7, 129.3, 129.1, 128.9, 127.9, 127.5, 127.4, 127.3, 127.0, 125.9, 125.4, 123.8, 123.5, 120.2, 110.9, 35.4, 31.2. MS (FAB) *m/z* 923 [M + 1]. HRMS (FAB) calcd. for $C_{68}H_{51}N_4$ $[M + H]^+$ *m/z* 923.4035; found 923.4115. Anal. Calcd for $C_{68}H_{50}N_4$: C, 88.47; H, 5.46; N, 6.07. Found: C, 88.09; H, 5.46; N, 6.06%.

Fabrication of OLEDs

The organic materials used for fabricating the devices were generally purified through high-vacuum, gradient temperature sublimation. The EL devices were fabricated through vacuum deposition of the materials at 10^{-6} torr onto glass precoated with a layer of ITO having a sheet resistance of 25 Ω square^{-1}. A LiF/Al cathode was deposited through sequential evaporation of LiF and Al metal. The electron-transporting material was TPBI or **BIAn**; the bilayer hole-transporting layers comprised NPB and TCTA. The effective area of the emitting diode was 3.1 mm^2. The current, voltage, and light intensity were measured simultaneously using a Keithley 2400 source meter and a Newport 1835-C optical meter equipped with a Newport 818-ST silicon photodiode. Electroluminescence spectra were measured using a Hitachi F-4500 fluorescence spectrophotometer.

Acknowledgements

We thank the National Science Council for funding and Professor C.-H. Cheng for his support during the preparation and characterization of the OLEDs.

References

1 C. Hosokawa, M. Eida, M. Matsuura, K. Fukuoka, H. Nakamura and T. Kusumoto, *Synth. Met.*, 1997, **91**, 3.
2 S. R. Forrest, P. E. Burrows, Z. Shen, G. Gu, V. Bulovic and M. E. Thompson, *Synth. Met.*, 1997, **91**, 9.
3 A. H. Tullo, *Chem. Eng. News*, 2001, **79**, 49.
4 T. Fuhrmann and J. Salbeck, *MRS Bull.*, 2003, **28**, 354.
5 L. S. Hung and C. H. Chen, *Mater. Sci. Eng. R.*, 2002, **39**, 143.
6 Y. S. Yao, Q. X. Zhou, X. S. Wang, Y. Wang and B. W. Zhang, *J. Mater. Chem.*, 2006, **16**, 3512.
7 B. J. Jung, J. I. Lee, H. Y. Chu, L. M. Lee and H. K. Shim, *J. Mater. Chem.*, 2005, **15**, 2470.
8 Q.-X. Tong, S.-L. Lai, M.-Y. Chan, Y.-C. Zhou, H.-L. Kwong and C.-S. Lee, *Chem. Phys. Lett.*, 2008, **455**, 79.

9 K. Okumoto, H. Kanno, Y. Hamaa, H. Takahashi and K. Shibata, *Appl. Phys. Lett.*, 2006, **89**, 063504.
10 C. H. Chen, F. I. Wu, C. F. Shu, C. H. Chien and Y. T. Tao, *J. Mater. Chem.*, 2004, **14**, 1585.
11 C. J. Tonzola, A. P. Kulkarni, A. P. Gifford, W. Kaminsky and S. A. Jenekhe, *Adv. Funct. Mater.*, 2007, **17**, 863.
12 N.-C. Seong, Y.-M. Jeon, T.-H. Lim, J.-W. Kim, C.-W. Lee, E.-J. Lee, J.-G. Jang, H.-J. Jang, J.-Y. Lee and M.-S. Gong, *Synth. Met.*, 2007, **157**, 421.
13 Y.-H. Kim, D.-C. Shin, S.-H. Kim, C.-H. Ko, H.-S. Yu, Y.-S. Chae and S.-K. Kwon, *Adv. Mater.*, 2001, **13**, 1690.
14 Y. Li, M. K. Fung, Z. Xie, S.-T. Lee, L.-S. Hung and J. Shi, *Adv. Mater.*, 2002, **14**, 1317.
15 K. Danel, T.-H. Huang, J. T. Lin, Y.-T. Tao and C.-H. Chuen, *Chem. Mater.*, 2002, **14**, 3860.
16 W.-J. Shen, R. Dodda, C.-C. Wu, F.-I. Wu, T.-S. Liu, H.-H. Chen, C. H. Chen and C.-F. Shu, *Chem. Mater.*, 2004, **16**, 930.
17 Y. Kan, L. Wang, L. Duan, G. Wu and Y. Qiu, *Synth. Met.*, 2004, **141**, 245.
18 D. Gebeyehu, K. Walzer, G. He, M. Pfeiffer, K. Leo, J. Brandt, A. Gerhard, P. Stößel and H. Vestweber, *Synth. Met.*, 2004, **141**, 245.
19 Y.-H. Kim, H.-C. Jeong, S.-H. Kim, K. Yang and S.-K. Kwon, *Adv. Funct. Mater.*, 2005, **15**, 1799.
20 Y.-Y. Lyu, J. Kwak, O. Kwon, S.-H. Lee, D. Kim, C. Lee and K. Char, *Adv. Mater.*, 2008, **20**, 2720.
21 I. B. Berlan, *Handbook of Fluorescence Spectra of Aromatic Molecules*, 2nd ed.; Academic Press: New York, 1971.
22 B. Balaganesan, W. J. Shen and C. H. Chen, *Tetrahedron Lett.*, 2003, **44**, 5747.
23 M. D. Joswick, I. H. Campbell, N. N. Barashkov and J. P. Ferraris, *J. Appl. Phys.*, 1996, **80**, 2883.
24 S. Tokito, H. Tanaka, K. Noda, A. Okada and Y. Taga, *Appl. Phys. Lett.*, 1997, **70**, 1929.
25 J. Salbeck, N. Yu, J. Bauer, F. Weissörtel and H. Bestgen, *Synth. Met.*, 1997, **91**, 209.
26 B. E. Konne, D. E. Loy and M. E. Thompson, *Chem. Mater.*, 1998, **10**, 2235.
27 Y. Shirota, *J. Mater. Chem.*, 2000, **10**, 1.
28 P.-I. Shih, C.-H. Chien, F.-I. Wu and C. F. Shu, *Adv. Funct. Mater.*, 2007, **17**, 3514.
29 R. C. Chiechi, R. J. Tseng, F. Marchioni, Y. Yang and F. Wudl, *Adv. Mater.*, 2006, **18**, 325.
30 B. K. Shah, D. C. Neckers, J. Shi, E. W. Forsythe and D. Morton, *Chem. Mater.*, 2006, **18**, 603.
31 D. Berner, C. Klein, M. K. Nazeeruddin, F. De Angelis, M. Castellani, Ph. Bugnon, R. Scopelliti, L. Zuppiroli and M. Graetzel, *J. Mater. Chem.*, 2006, **16**, 4468.
32 S.-K. Kim, B. Yang, Y. Ma, J.-H. Lee and J.-W. Park, *J. Mater. Chem.*, 2008, **18**, 3376.
33 S.-K. Kim, Y.-I. Park, I.-N. Kang and J.-W. Park, *J. Mater. Chem.*, 2007, **17**, 4670.
34 T. Ishiyama, M. Murata and N. Miyaura, *J. Org. Chem.*, 1995, **60**, 7508.
35 B. Balaganesan, W. J. Shen and C. H. Chen, *Tetrahedron Lett.*, 2003, **44**, 5747.
36 P. I. Shih, C. H. Chien, C. Y. Chuang, C. F. Shu, C. H. Yang, J. H. Chen and Y. C. Tsai, *J. Mater. Chem.*, 2007, **17**, 1692.
37 J. Shi and C. W. Tang, *Appl. Phys. Lett.*, 2002, **80**, 3201.
38 B. Ding, W. Zhu, X. Jiang and Z. Zhang, *Curr. Appl. Phys.*, 2008, **8**, 523.
39 S. Tao, Z. Hong, Z. Peng, W. Ju, X. Zhang, P. Wang, S. Wu and S. Lee, *Chem. Phys. Lett.*, 2004, **397**, 1.
40 S. Tao, Z. Peng, X. Zhang, P. Wang, C.-S. Lee and S.-T. Lee, *Adv. Funct. Mater.*, 2005, **15**, 1716.
41 P. I. Shih, C. Y. Chuang, C. H. Chien, E. W. G. Diau and C. F. Shu, *Adv. Funct. Mater.*, 2007, **17**, 3141.
42 Z. Q. Gao, Z. H. Li, P. F. Xia, M. S. Wong, K. W. Cheah and C. H. Chen, *Adv. Funct. Mater.*, 2007, **17**, 3194.
43 M.-H. Ho, Y.-S. Wu, S.-W. Wen, T.-M. Chen and C. H. Chen, *Appl. Phys. Lett.*, 2007, **91**, 83515.
44 V. K. Tandon and M. Kumar, *Tetrahedron Lett.*, 2004, **45**, 4185.

